JBC Papers in Press. Published on February 26, 2018 as Manuscript RA118.001875
The latest version is at http://www.jbc.org/cgi/doi/10.1074/jbc.RA118.001875

# SbnI is a free serine kinase that generates *O*-phospho-L-serine for staphyloferrin B biosynthesis in *Staphylococcus aureus*

**Meghan M. Verstraete[1], Cecilia Perez-Borrajero[2], Kirstin L. Brown[1], David E. Heinrichs[3], Michael E. P. Murphy[1]***

From the [1]Department of Microbiology and Immunology, [2]Genome Sciences and Technology Program Life Sciences Institute, University of British Columbia, Vancouver, BC, V6T 1Z3, Canada; [3]Department of Microbiology and Immunology, University of Western Ontario, London, ON, N6A 5C1, Canada

Running title: *SbnI serine kinase activity and role in SB biosynthesis*

*To whom correspondence should be addressed: Michael E. P. Murphy, Department of Microbiology and Immunology, 2350 Health Sciences Mall, The University of British Columbia, Vancouver, BC, Canada, V6T 1Z3; Telephone: (604) 822-8022; E-mail: michael.murphy@ubc.ca

**Keywords:** *Staphylococcus aureus* (*S. aureus*), siderophore, kinase, crystal structure, kinetics, *O*-phospho-L-serine, staphyloferrin, virulence factor

## ABSTRACT

Staphyloferrin B (SB) is an iron-chelating siderophore produced by *Staphylococcus aureus* in invasive infections. Proteins for SB biosynthesis and export are encoded by the *sbnABCDEFGHI* gene cluster, in which SbnI, a member of the ParB/Srx superfamily, acts as a heme-dependent transcriptional regulator of the *sbn* locus. However, no structural or functional information about SbnI is available. Here, a crystal structure of SbnI revealed striking structural similarity to an ADP-dependent free serine kinase, SerK, from the archaea *Thermococcus kodakarensis*. We found that features of the active sites are conserved, and biochemical assays, and $^{31}$P NMR and HPLC analyses indicated that SbnI is also a free serine kinase but uses ATP rather than ADP as phosphate donor to generate the SB precursor *O*-phospho-L-serine (OPS). SbnI consists of two domains, and elevated B-factors in domain II were consistent with the open-close reaction mechanism previously reported for SerK. Mutagenesis of Glu20 and Asp58 in SbnI disclosed that they are required for kinase activity. The only known OPS source in bacteria is through the phosphoserine aminotransferase activity of SerC within the serine biosynthesis pathway and we demonstrate that an *S. aureus serC* mutant is a serine auxotroph, consistent with a function in L-serine biosynthesis. However, the *serC* mutant strain could produce SB when provided L-serine, suggesting that SbnI produces OPS for SB biosynthesis *in vivo*. These findings indicate that besides transcriptionally regulating the *sbn* locus, SbnI also has an enzymatic role in the SB biosynthetic pathway.

*Staphylococcus aureus* is a prominent human pathogen that also asymptomatically colonizes a proportion of the human population (1, 2). Though colonization is typically not harmful to the host, *S. aureus* is frequently associated with minor skin and soft tissue infections. In more serious cases, it is capable of breaching host innate immune responses to gain access to deep tissues causing more severe and invasive infections including endocarditis, osteomyelitis, and necrotizing pneumonia (2, 3).

Successful iron uptake from the human host is integral to infection and pathogenesis of *S. aureus* and most other microbial pathogens (4, 5). Iron is reactive and tightly regulated in the human body to restrict toxicity and to limit bioavailability to invading microbial pathogens as a type of innate, nutritional immunity (6). As such, iron in the mammalian host is found either within heme and bound to hemeproteins,

intracellularly bound to proteins as free ions or iron-sulfur clusters, stored in ferritin, or extracellularly complexed with glycoproteins like transferrin (7, 8). *S. aureus* has evolved several mechanisms to counter iron restriction and exploit a variety of host iron sources. Iron uptake strategies employed include heme uptake via the iron-responsive surface determinant (Isd) system and through synthesis and secretion of two iron-chelating siderophores, staphyloferrin A (SA) and staphyloferrin B (SB) (9–11). Siderophores are small molecules with high iron affinity capable of outcompeting extracellular host iron-binding proteins for ferric iron. Iron-bound siderophores are selectively imported by dedicated surface receptors and cognate ABC transporters, HtsABC and SirABC for SA and SB, respectively (12).

SA and SB have both been implicated in pathogenesis of *S. aureus* but SB has been recognized for its importance in severe disease phenotypes and promotion of staphylococcal virulence in abscess and endocarditis models of infection (13, 14). Additionally, the SB biosynthetic locus and *sirABC* are amongst the most strongly up-regulated genes in bacteria isolated from the iron-restricted host (15–17). Importantly, SB biosynthesis can occur independent of TCA cycle activity, which is down-regulated in *S. aureus* as part of the iron-sparing response (18, 19). In contrast, SA biosynthesis is dependent on the TCA cycle for citrate precursors (18).

Staphyloferrin biosynthesis is achieved through Non-ribosomal peptide synthetase-Independent Siderophore (NIS) biosynthesis (20, 21). NIS synthesis systems involve intermediates and enzymes that are freely dissociable from each other during assembly. Primary metabolites generally serve as the source of building blocks to generate siderophores and can be first chemically modified prior to incorporation into the siderophore. In addition to the synthetases required for assembly of the siderophore, NIS biosynthetic gene clusters generally encode enzymes that synthesize the necessary precursors to be assembled by the NIS synthetases (22).

The SB biosynthetic operon consists of nine genes, *sbnABCDEFGHI*. SbnC, SbnE, and SbnF are the three synthetases and SbnH is a decarboxylase that together are required for SB assembly from one molecule of each α-ketoglutarate (α-KG) and citrate, and two molecules of L-2,3-diaminopropionate (L-Dap) (21). These essential precursor molecules are synthesized by SbnA, SbnB, and SbnG. SbnG is a dedicated citrate synthase that produces citrate from oxaloacetate and acetyl-CoA (18, 23, 24). α-KG and L-Dap are provided by the sequential enzymatic activities of SbnA and SbnB which use substrates O-phospho-L-serine (OPS) and L-glutamate (25, 26). OPS is postulated to be shunted from the serine biosynthesis pathway stemming from 3-phosphoglycerate produced in glycolysis (Fig. 1) (18, 26).

SbnI, the ninth gene product, is a heme-responsive transcriptional regulator for SB production (27). SbnI is required for full expression of *sbnD-H* and thus controls SB-mediated iron acquisition. SbnI binds a 271-bp DNA fragment in the *sbnC* coding region. However, SbnI can bind heme which abrogates interaction with DNA thereby limiting SB production. A model is proposed by which SbnI is required for transcription of the full SB biosynthetic operon and senses heme to reduce SB synthesis in favor of heme acquisition (27). This model also provides a mechanism for the findings that *S. aureus* demonstrates a heme-iron preference *in vitro* (28).

Based on primary sequence analysis, homology was not detected between SbnI and any characterized transcription factors or heme-binding proteins (27), but it is annotated as containing an N-terminal ParB-like domain. ParB is an essential component of the chromosome segregation system in bacteria (29). However, the conserved N-terminal ParB-like domain in SbnI is not responsible for interaction with DNA in ParB (30), leaving the role of the ParB-like domain in SbnI unknown.

The aim of this study was to gain insight into how SbnI functions using X-ray crystallography. The SbnI structure revealed striking structural homology to a recently characterized free serine kinase, SerK, from the archaea *T. kodakarensis* (31). SerK can phosphorylate free L-serine using ADP to generate OPS for cysteine biosynthesis (32). Herein, we demonstrate that SbnI is also a free serine kinase that uses ATP to phosphorylate L-serine to yield OPS and ADP (Fig. 1). The structure of SbnI, supported by site-directed

mutagenesis, suggests that it follows a similar open-close reaction mechanism as proposed for SerK. Additionally, SbnI-generated OPS can be used by SbnA *in vitro* and serves as the *in vivo* source of OPS for SB production. To our knowledge, this is the first example of a bacterial free serine kinase and the first described free serine kinase that is ATP dependent. This enzymatic function earns SbnI an enzymatic role in the SB biosynthetic pathway in addition to its heme-dependent transcriptional regulatory function.

## Results

### *Structure determination of SbnI*

Full length (254 amino acid) SbnI was not amendable for X-ray crystallography due to its propensity to precipitate. To improve solubility and stability in solution, several expression constructs were made containing varying N- and C-terminal truncations based on predicted secondary structure and disorder identified using PSIPRED and DISOPRED, respectively (33, 34). One construct containing a 14-amino acid C-terminal truncation, SbnI$^{1-240}$, had improved stability in solution and produced well-diffracting crystals. The structure of selenomethionine-labelled SbnI$^{1-240}$ was determined to 2.5 Å resolution using single wavelength anomalous dispersion in space group $P3_1$with one molecule in the asymmetric unit (Fig. 2A). Data collection and refinement statistics are summarized in Table 1. All 240 residues were modeled with 98% of residues in the most favored regions of the Ramachandran plot.

SbnI$^{1-240}$ is comprised of two domains, domain I and domain II. Domain I consists of residues M1-Q83 and I205-A240 and domain II is composed of residues Y84-N204. Domain I includes a conserved core ParB/Srx fold, corresponding to the annotated ParB-like domain based on primary sequence. This fold has been described in a functionally diverse ParB/Srx superfamily of proteins. Members are found in varied biological contexts and thus far are described to bind a nucleotide for kinase, ATPase, or DNase activity (35, 36). To our knowledge, no ParB/Srx family member has been found to be directly involved in siderophore biosynthesis. The ParB/Srx core domain is comprised of a 4-strand mixed β-sheet and two α-helices, α2 and α3 (Fig. 2A) and contains an absolutely conserved GXXR motif, GVHR$^{59-62}$ in SbnI.

Domain II is composed of a mixed α/β fold with a central 4-stranded antiparallel β-sheet surrounded by 5 α-helices. A pair of antiparallel β-strands abut the main sheet and serve as a linker to Domain I. B-factor analysis reveals that domain II has a relatively high average B-factor of 109 Å$^2$, compared to 75 Å$^2$ in domain I, suggesting domain II has more disorder in the crystal and the domains are connected by a flexible linker.

To gain functional insight into SbnI, a search of the SbnI$^{1-240}$ structure against structures in the PDB was performed with the Dali server. Five proteins all belonging to the functionally diverse superfamily of ParB/Srx proteins were identified (Z score < 3.9). The most striking observation was the high structural similarity SbnI shared with the top search result, SerK (PDB ID: 5X0B). Superimposition of SbnI$^{1-240}$ with SerK (PDB ID: 5X0B) using PDBeFOLD has a root mean square distance (RMSD) of 2.0 Å for 194 Cα despite sharing only 19% amino acid sequence identity across the aligned residues (Fig. 2B). The other structures also share modest sequence identity (12-23%) and include sulfiredoxin (Srx) from *Homo sapiens* (PDB ID: 2RII, RMSD of 2.7 Å across 84 residues), chromosome partitioning protein (ParB) from *Sulfolobus solfactaricus* (PDB ID: 5K5D, RMSD of 2.5 Å across 71 residues), oncogenic suppressor (Osa) from *Shigella flexneri* (PDB ID: 4OVB, RMSD of 3.7 Å across 83 residues), and chromosome segregation protein (Spo0J) from *Thermus thermophilus* (PDB ID: 1VZ0, RMSD of 5.4 Å across 76 residues) (31, 36–39).

SerK is a free serine kinase from *T. kodakarensis* that uses ADP to phosphorylate L-serine to generate OPS for cysteine biosynthesis. Of the proteins annotated in the ParB/Srx family, SerK is the only identified kinase though Osa and Srx both possess ATPase activity (36, 40). Overall, the structures of SerK and SbnI are very similar. The SerK domain II has a high average B-factor and superimposition of SbnI$^{1-240}$ with the SerK structure in a "closed" conformation (PDB ID: 5X0E) suggests how SbnI may possess similar domain flexibility in solution (Fig. 2C). Additionally, structural superimposition and

multiple sequence alignments revealed that several residues important for substrate and product binding identified in the SerK crystal structure (PDB ID: 5X0E) are conserved in SbnI. Moreover, the active site architecture is highly conserved between the two proteins (Fig. 2D, Fig. S1). Of the active site residues, SerK Glu30 was identified as a catalytically essential residue and Asp69 is required for magnesium ion binding; site-directed mutagenesis of either of these residues abolished SerK kinase activity (31). The homologous residues in SbnI are Glu20 and Asp58.

The genomic context of *sbnI* was analysed to compare with the genomic neighborhoods of homologs. All staphylococcal *sbnI* homologs are part of the nine gene SB biosynthetic cluster. More distant homologs co-occur with *sbnA* and *sbnB* homologs, either alone or in combination with different putative siderophore biosynthetic enzymes (Fig. 3). More distant SbnI homologs are shorter and alignments suggests that they have an abbreviated domain II (Fig. S1). Interestingly, a putative *sbnI* ortholog was identified upstream of the *sbnA-H* gene locus in *Ralstonia solanacearum*, which was previously thought to lack a SbnI homolog but still produces SB (41). A multiple sequence alignment of SerK and SbnI homologs used in the genomic neighborhood analysis reveals that certain key residues important for catalysis, substrate, and product binding identified in SerK are fully conserved (Fig. S1). Notably, these include the SerK catalytic residue Glu30, magnesium ion binding residue Asp69, residues implicated in interacting with the β phosphate of ADP or phosphate group of OPS, His72 and Arg73, and residues that interact with the serine moiety of OPS, Trp102 and Thr223 (Fig. S1). More variability is seen with the SerK residues interacting with the adenosine group, raising the possibility that SbnI and other homologs may use a different phosphate donor or binding-mode. Overall, the genomic neighborhood and sequence analyses suggest that free serine kinases are found in diverse species belonging to Firmicute and Proteobacteria phyla.

Consurf analysis of $SbnI^{1-240}$ was used to map conserved regions to the molecular surface (Fig. 4). Highly conserved residues including those that form the kinase active site delineate a groove between domain I and II (Fig. 4AB). Structural alignment with the structure of the SerK ternary product complex (PDB ID: 5X0E) revealed that among SbnI homologs, the putative active site is highly conserved, while the remainder of the protein surface is variable (Fig. 4C).

***SbnI is a dimer in solution***

The oligomeric state of SbnI was analyzed using dynamic light scattering (DLS). Since SbnI contains 7 Cys residues, the analysis was conducted in the presence of GSH as a reductant. The calculated molecular weight based on amino acid sequence of full-length SbnI is 30 kDa and the measured molecular weight by DLS was 61 ± 6 kDa with an average of 24 ± 7% of polydispersity, implying it predominantly forms a dimer in solution (Fig. S2). The molecular weight of $SbnI^{1-240}$ by DLS was 28 ± 3 kDa with 34 ± 1% polydispersity (Fig. S2). $SbnI^{1-240}$ has a calculated weight of 28 kDa, implying it is primarily a monomer in solution. These data indicate that the C-terminal 14 amino acids excluded from the $SbnI^{1-240}$ construct are important for dimerization of the full-length protein.

***SbnI is a serine kinase that uses L-serine and ATP to generate OPS***

OPS is a substrate for SbnA in SB biosynthesis (25, 26), lending support to our hypothesis that SbnI produces OPS for use by SbnA. To thus test if SbnI is capable of producing OPS, the spectral changes that occur when SbnA binds OPS were used to assay SbnI activity. SbnA has a characteristic absorption maxima at 412 nm attributed to an internal Schiff base formed between its pyridoxal 5'-phosphate (PLP) cofactor and an active site lysine. Adding OPS to SbnA causes a rapid change in UV-Vis spectra with the appearance of absorption peaks at 324 nm and 467 nm (Fig. 5A), characteristic of the formation of an external aminoacrylate intermediate (25). This spectral change is specific to OPS and does not occur with *O*-acetyl-L-serine or L-serine (25). SbnA incubated with SbnI, L-serine, and ADP resulted in no change in the UV-Vis spectrum of SbnA. However, SbnA incubated with SbnI, L-serine, and ATP led to a shift in the UV-Vis spectra indicative of OPS production and reaction with SbnA-PLP to form the external

aminoacrylate (Fig. 5BC). No spectral change was observed when SbnI was omitted indicating that only the SbnI enzymatic product could react with SbnA-PLP. Therefore, we conclude that the reaction product is most likely OPS and SbnI activity is ATP-dependent.

Phosphate acceptors, alternative to L-serine, were tested using a pyruvate kinase/lactate dehydrogenase (PK/LDH) assay for detection of ATP conversion to ADP. L-threonine, α-KG, and L-Dap were not phosphate acceptors (data not shown). Additionally, SbnI did not phosphorylate the serine residue in a His-Ser dipeptide (data not shown).

SbnI-mediated conversion of ATP to ADP and generation of OPS were monitored using HPLC and $^{31}$P NMR. Incubation of SbnI with ATP and excess L-serine led to turnover of ATP to ADP as detected by HPLC (Fig. 6A) indicating SbnI has ATPase activity. Unlike SerK, no turnover of ADP to AMP was detected with ADP as a phosphate donor by HPLC (Fig. 6A). ADP was not generated with when L-serine was excluded, indicating that this activity requires the presence of L-serine. $^{31}$P NMR was also used to monitor SbnI-mediated ATPase activity and generation of OPS from L-serine. The observed disappearance of the ATP γ-phosphate $^{31}$P signal with the concomitant appearance of a $^{31}$P signal of OPS demonstrates transfer of the ATP γ-phosphate to L-serine to yield ADP and OPS (Fig. 7). The chemical shift of SbnI-generated OPS was consistent with the $^{31}$P NMR spectrum measured for an OPS standard (Fig. S3). Attempts to obtain a co-crystal structure of SbnI with identified substrates (or ATP analog, adenyl-imidodiphosphate) or products, both in the presence and absence of heme, have not been met with success.

***SbnI active site variants***

The role of Glu20 and Asp58 in SbnI kinase function were tested by site-directed mutagenesis. Two mutants each containing a single alanine substitution, SbnI E20A and SbnI D58A, were generated. Using the PK/LDH assay, we determined that the mutants were incapable of turning over ATP to ADP in the presence of L-serine. Additionally, no ADP could be detected by HPLC in reactions containing the SbnI mutants incubated with ATP and L-serine (Fig. 6B); together, these data allow us to conclude that these mutants are catalytically inactive. These data also correlate with SbnA-PLP UV-Vis absorption spectra that demonstrated that these SbnI variants also do not produce OPS (Fig. 5DE). The importance of these residues in catalysis is consistent with the reaction mechanism presented for SerK in which substrate binding promotes conformational closure positioning the catalytic Glu30 (Glu20 in SbnI) close to the hydroxyl group of bound L-serine. Glu30 is a catalytic base that deprotonates the hydroxyl group of L-serine. The deprotonated hydroxyl can then attack the phosphorus atom of the ADP β-phosphate to yield OPS and AMP (31). Our results suggest SbnI uses a similar two-ligand binding sequential mechanism, but instead uses L-serine and ATP to yield ADP and OPS.

***Kinetic analysis of SbnI kinase activity***

To obtain kinetic parameters for the SbnI kinase activity, SbnI enzymatic turnover was monitored using an established coupled assay for ADP using PK/LDH. The steady-state kinetic parameters of SbnI reaction with ATP and L-serine were determined and are summarized in Table 2. The saturating concentration of L-serine was beyond conditions permissive to the assays and thus $K_m$ could not be accurately determined. A second assay to measure SbnI enzymatic turnover employed SbnA-dependent turnover of OPS coupled to a phosphate release detection assay. SbnA is the most likely *in vivo* acceptor of OPS generated by SbnI to facilitate synthesis of SB substrates L-Dap and α-KG, in concert with SbnB. Using excess concentrations of SbnA, the coupled assay demonstrated that SbnA could use SbnI-generated OPS and supplied L-glutamate to generate its products, *N*-(1-amino-1-carboxyl-2-ethyl)-glutamic acid and inorganic phosphate. The kinetic parameters of SbnI reaction with ATP and L-serine using the SbnA coupled assay were determined and are summarized in Table 2. The kinetic parameters measured using both methods agree with rates and $K_m$ values in the same order of magnitude. SbnI mutants E20A and D58A were catalytically insufficient to accurately measure enzyme rates. Compared to SerK, SbnI has a $K_m$ for ATP one order of magnitude lower than SerK has for ADP and a higher $K_m$ for L-serine by 2-orders of magnitude.

The enzymatic activity of SbnI$^{1-240}$ was also measured since the 14-amino acid C-terminal truncation does not exclude any regions in the SerK structures identified as required for substrate and product binding or catalysis. SbnI$^{1-240}$ displayed decreased kinase activity compared to full-length SbnI. These data correlate with the HPLC and spectral data with SbnA for SbnI$^{1-240}$ having intermediate activity relative to full-length SbnI (Fig. 5F, 6B). Plots of initial velocities used for determination of kinetic constants are included in the supporting information (Fig. S4). Given that SbnI$^{1-240}$ is a monomer in solution (see above), we conclude that dimerization/ oligomerization of SbnI is not essential for its kinase activity.

***Physiological function of ATP-dependent serine kinase activity in S. aureus***

The *serC* gene encodes the enzyme responsible for OPS synthesis from 3-phosphohydroxypyruvate in the *S. aureus* serine biosynthesis pathway. To our knowledge, prior to this work, SerC activity was the only identified metabolic source of OPS in *S. aureus* and was the assumed source of OPS for SB biosynthesis (18, 26). To test if other metabolic sources of OPS exist in *S. aureus*, wildtype USA300 and a *serC* transposon insertion mutant USA300 strain (*serC*) were grown in chemically defined media containing glucose with and without L-serine in a TECAN plate reader. In L-serine replete medium, both wildtype USA300 and the *serC* mutant grew, although the *serC* mutant entered stationary phase at a lower cell density and failed to reach equivalent biomass as that of the WT culture (Fig. 8A). However, in stark contrast, in a growth medium lacking L-serine, wildtype USA300 grew while the *serC* mutant failed to grow altogether (Fig. 8A). Thus, we conclude that the *serC* transposon mutant is a *bona fide* serine auxotroph; a serine auxotrophy phenotype was previously observed for an *Escherichia coli serC* mutant strain (42). We also conclude that SerC activity is the sole source of OPS for serine biosynthesis; since the medium is iron-restricted, SbnI would be expressed and, if it contributed to OPS biosynthesis for use in the L-serine biosynthetic pathway, we would have not observed L-serine auxotrophy for the *serC* mutant (see Fig. 1).

To test if SbnI could serve as a source of OPS for SB biosynthesis, the *serC* transposon insertion mutant was tested for its ability to make SB. A disc diffusion assay was used to detect SB in spent culture supernatant of *serC* and *sbnI* transposon insertion mutants, compared to the wildtype USA300 *S. aureus* strain. Briefly, spent culture supernatants were applied to sterile filter discs on iron-restricted agar seeded with either *sirA* or *htsABC* mutant *S. aureus* strains. The *sirA* mutant strain is defective for SB uptake so growth promotion around the disc in iron-restricted media is dependent on the presence of SA in the supplied culture supernatant. The *htsABC* mutant strain is unable to take up SA and thus growth around the disc is reliant on the presence of SB in supplied culture supernatant. Similar to wildtype *S. aureus*, the *serC* transposon insertion mutant was capable of producing SB (Fig. 8B), indicating the presence of another pathway for OPS production independent of SerC, almost assuredly via SbnI (Fig. 1).

The *sbnI* mutant was impaired for SB production (Fig. 8B), consistent with previously published results using the disc diffusion assay (27). Decreased SB production by the *sbnI* mutant is due to the necessity of SbnI for full expression of *sbnDEFGH* (27). A *serC sbnI* double mutant is expected to be SB deficient. However, as the *sbnI* mutation is pleiotropic on SB biosynthesis due to its requirement for transcription of *sbn* biosynthetic genes, assaying for SB production does not inform on a role in OPS production. Nonetheless, our results support the hypothesis that SbnI serves as a second metabolic route for OPS biosynthesis from L-serine in *S. aureus*. Production of OPS from L-serine and ATP is a previously unrecognized route for OPS synthesis in bacteria.

**Discussion**

SbnI is a free L-serine kinase that makes OPS, which serves as a substrate for SbnA and is a precursor for SB biosynthesis. Insight into the kinase function of SbnI was gained based on homology identified by structural similarity with SerK, an enzyme in a biosynthetic pathway for cysteine in the thermophilic archaea *T. kodakarensis* (31). ATP is used as the phosphate donor in the reaction catalysed by SbnI, whereas SerK uses ADP. Interestingly, hyperthermophiles

generally use ADP in place of ATP in key glycolytic enzymes as an adaptation to life at high temperatures, presumably because ADP is more stable than ATP (43). While SbnI is capable of phosphorylation of free L-serine, it was not capable of mediating phosphotransfer to serine residues within a His-Ser dipeptide. Bacterial Ser/Thr kinases such as *S. aureus* Stk1 (also named PknB) (44) and cognate phosphatases function as molecular switches that have key roles in bacterial cell signaling as in eukaryotic systems (45). However, SbnI free L-serine kinase activity is functionally and enzymatically distinct from that of Ser/Thr kinases.

SbnI$^{1\text{-}240}$ retained partial catalytic efficiency compared to full-length SbnI. As SbnI$^{1\text{-}240}$ is lacking 14 residues at the C-terminus and is monomeric, either the C-terminus or dimerization is required for full kinase function. The residues shown to be required for phosphotransfer in SerK (Glu30, Asp69) are conserved in SbnI and present in the truncated protein. Moreover, three of four residues interacting with the serine substrate in SerK are conserved (Glu30, Trp102, Thr223) and the fourth position is a conservative substitution of His225 with Phe203 in SbnI (Fig. 2D). In contrast, interactions of SerK with ADP/AMP are poorly conserved. Of eight residues making key contacts, only three residues (Ser43, His72, Arg73) are conserved in SbnI and two of these interact with the phosphate groups. Attempts to obtain crystals with substrates or products bound to SbnI or SbnI$^{1\text{-}240}$ have not been met with success and the binding mode of ATP to SbnI remains elusive.

Structural analysis of SerK suggests that the conformational closure upon binding both substrates positions the catalytic glutamate (Glu30) to deprotonate L-serine to attack the terminal phosphate of ADP. With no published structure of substrate or product-free SerK, the apo-SbnI$^{1\text{-}240}$ structure supports this proposed mechanism in that the unbound form is in an open conformation to expose the binding pocket. Measurement of SbnI enzyme kinetic parameters revealed that, compared to SerK, it has a relatively low selectivity for L-serine. The comparatively low $k_{cat}/K_m$ could relate to the physiological role of SbnI in *S. aureus*. SerK supplies cysteine synthase with OPS to produce cysteine and may represent an ancient heterotrophic mechanism of amino acid metabolism (35). Interestingly, this cysteine synthase is a distant SbnA homolog and a true OPS sulfhydrylase. Also, SerK is postulated to provide an advantage by enabling carbon from serine to be directed to glycolysis and gluconeogenesis by conversion to OPS (35). *In vitro* evidence suggests that *S. aureus* uses amino acids to support gluconeogenesis (46). However, serine is used to generate ATP and acetate rather than to facilitate gluconeogenesis as in *T. kodakarensis* (35, 46). In contrast, SbnI kinase activity fulfils a distinct physiological role, providing substrate necessary for SB production. The comparatively low $k_{cat}/K_m$ may allow SbnI to respond to a greater range of substrate concentrations, such that at high L-serine concentrations SbnI increases the rate of OPS production for SB production and possibly other metabolic processes. Though SbnI has lower catalytic efficiency than SerK (Table 2), the related ParB/Srx family member, Srx, is similar to SbnI as it is not a highly efficient enzyme. The Srx ATP-dependent reduction of peroxidreoxin sulfinic acid activities described in mammals and plants so far are slow, with turnover rates of 0.2-0.5 min$^{-1}$ for ATP, which are an order of magnitude lower than SbnI (47–49). However, the catalytic efficiencies of Srx are 0.8-8.4 mM$^{-1}$ min$^{-1}$ and in the range measured for SbnI (47, 49).

SbnI is a sufficient biological source of OPS for SB biosynthesis and contributes to the functional modularity of the *sbn* locus. A recognized characteristic of bacterial networks is a high degree of modularity and sparse connectivity between individual functional modules, where a functional module refers to a group of biological components that are spatially isolated or chemically specific and work together for a discrete biological function (50). The functional redundancy of enzymes encoded in the *sbn* locus for generation of precursor substrates, SbnG and SbnI, decreases dependence on central metabolism and contribute to the modularity of the *sbn* locus. SbnG is functionally redundant with the TCA cycle citrate synthase, CitZ (23). Moreover, SbnG activity allows for SB biosynthesis to occur independent of TCA cycle activity (18). This functional independence is important because *S. aureus* elicits an iron-sparing response during infection resulting in

down-regulation of the TCA cycle. We propose that the functional redundancy of SbnI with SerC for OPS production allows SB biosynthesis to occur independent of glycolysis as SerC substrate is funneled from 3-phosphoglycerate. Additionally, the serine biosynthetic pathway is regulated by negative feedback where SerA, metabolically upstream of SerC, is allosterically inhibited by L-serine and could limit the amount of SerC-derived OPS available to support SB synthesis when serine is abundant. Thus, an alternative, SB-dedicated, OPS synthetic route via SbnI is advantageous. Together with SbnG, SbnI allows SB biosynthesis to occur autonomously from glycolysis and TCA cycle activity by generating precursor substrates dedicated to SB biosynthesis.

This observed metabolic redundancy may improve robustness and help buffer environmental perturbations *S. aureus* encounters during infection. Glucose is the preferred carbon source by *S. aureus* and available at concentrations to support growth in human blood (51). However, within staphylococcal abscesses, glucose is limiting and *S. aureus* likely survives through catabolism of secondary carbon sources, specifically lactate, peptides, and free amino acids (46, 52, 53). Resultant changes in central metabolism of *S. aureus* may not severely hinder SB biosynthesis due to the modularity of the *sbn* system. Despite variability in growth conditions, one constancy in *S. aureus* survival strategy is iron acquisition.

Serine is amongst the most abundant amino acids found in fluid obtained from *S. aureus* infected prosthetic joints. SB biosynthetic genes including *sbnI*, but not SA biosynthetic genes, are up-regulated in this environment (17). Also, L-serine is one of the most rapidly consumed amino acids by *S. aureus* grown on amino acids *in vitro* (46). Together, the combination of high L-serine in the extracellular milieu and the rapid consumption of L-serine may limit the activity of the endogenous serine biosynthetic pathway. Under these conditions OPS from serine biosynthesis is likely to be limiting to feed SB biosynthesis justifying the necessity of SbnI-generated OPS. Interestingly, SB production is restricted to more invasive coagulase-positive staphylococcal strains and the *sbn* locus may represent a lineage-specific innovation to support adaptation to a more invasive lifestyle. In contrast, SA biosynthetic genes are found across both coagulase-positive staphylococci and more commonly commensal coagulase-negative staphylococci.

This newly determined enzymatic role of SbnI generates questions regarding how it carries out heme-dependent transcriptional regulation of the *sbn* locus. It remains unclear if SbnI kinase activity impacts its heme-dependent transcriptional regulation of the *sbn* locus. The structure of $SbnI^{1-240}$ did not reveal a prototypical DNA-binding motif or heme binding site. The functional sites required for kinase activity could be structurally distinct from those involved in the transcriptional regulation and heme-binding. Full-length SbnI is a dimer yet $SbnI^{1-240}$ is a monomer in the crystal structure and in solution. The C-terminal 14 amino acids excluded from the $SbnI^{1-240}$ construct are likely required for multimerization, which could be important for transcriptional regulatory function or heme-binding. Additionally, SbnI has a C-terminal extension of 34 amino acids compared to SerK and this C-terminal region is truncated in distant SbnI homologs not associated with a SB biosynthetic locus. This raises the possibility that kinase activity may be the core function of the non-SB-associated SbnI homologs. The C-terminal extension in SbnI could be a structural adaptation to facilitate multiple biological functions in SB precursor biosynthesis and *sbn* locus gene regulation. Heme-dependent SbnI regulatory activity may further enhance network robustness as a negative feedback loop from an iron acquisition perspective. Characterization of SbnI heme-binding and effect on kinase activity remains the subject of future work.

OPS production by the kinase activity of SbnI represents a new biosynthetic path for production of this metabolite in bacteria. SbnI may serve as a metabolic adaptation to facilitate SB production when growing on non-preferred carbon sources. Furthermore, it demonstrates the metabolic flexibility *S. aureus* possesses to allow employment of iron uptake strategies in changing host environments.

## Experimental procedures

### *Cloning and site-directed mutagenesis*

Constructs with an N-terminal $His_6$ tag and thrombin cleavage site were generated in pET28a vectors for recombinant expression of *S. aureus* full-length SbnI, residues 1-254, with the first codon mutated from the native TTG to a common start codon, ATG, and the *S. aureus* C-terminal truncated construct $SbnI^{1-240}$ (residues 1-240). The *S. aureus* SbnI nucleotide sequence can be accessed in the GenBank database under accession code NC_009641.1 (90178-90942) (gene locus NWMN_RS00380) and the amino acid sequence can be accessed through NCBI Protein Database under NCBI accession WP_001015549.1. Briefly, a megaprimer-based whole-plasmid synthesis PCR cloning protocol was used to clone constructs amplified from chromosomal DNA from *S. aureus* strain Newman (54). *S. aureus* SbnI variants E20A and D58A were produced using a single primer mutagenesis method (55). Primers used in this study are summarized in Table S1. All clones were introduced into *E. coli* BL21 (λDE3) and confirmed by DNA sequencing. Bacterial strains and plasmids used in this study are summarized in Table 3.

***Protein expression and purification***

Recombinant full-length SbnI, $SbnI^{1-240}$, SbnI E20A, and SbnI D58A constructs were overexpressed in *E. coli* BL21 (λDE3) cells. Cultures were grown in 2xYT media supplemented with 25 μg/mL kanamycin at 30°C to an $OD_{600}$ of 0.7-0.9. Cultures were then induced with 0.5 mM isopropyl β-D-thiogalactopyranoside and grown for an additional 18 h at 20°C. Cells were pelleted by centrifugation at 4400 x g for 7 min at 4 °C and resuspended in buffer containing 50 mM HEPES (pH 7.4), 300 mM NaCl, 5% (v/v) glycerol, 2 mM tris(2-carboxyethyl)phosphine (TCEP), and 10 mM imidazole on ice. Approximately 5 mg of DNase was added to cell suspension prior to lysis at 4°C using an EmulsiFlex-C5 homogenizer (Avestin). Insoluble material was removed by centrifugation at 39,000 x g for 1 h and recombinant protein was purified from soluble lysate using a HisTrap nickel affinity column (GE Healthcare) by elution with an imidazole gradient. Protein was dialyzed against 50 mM HEPES (pH 7.4), 100 mM NaCl, 5% (v/v) glycerol, and 2 mM TCEP and then cleaved with thrombin at a 1:500 ratio by weight of $His_6$ protein to remove the $His_6$ tag over 18 hr at 4°C. Subsequently, recombinant protein was dialysed into 50 mM HEPES (pH 7.4), 5% (v/v) glycerol, and 2 mM TCEP and further purified by anion exchange chromatography using a Source 15Q column (GE Healthcare). Purified protein was obtained by elution with a NaCl gradient and further dialyzed into 50 mM HEPES (pH 7.4), 300 mM NaCl, 5% (v/v) glycerol, 2 mM GSH. The sample was concentrated to approximately 20 mg/mL, flash frozen, and stored at -80°C. Selenomethionine-incorporated $SbnI^{1-240}$ was produced by methods previously described (56) and purified as described above for native $SbnI^{1-240}$.

$His_6$-tagged SbnA was expressed in *E. coli* BL21 (λDE3) cells from the plasmid pET28a, purified by His-tag affinity chromatography, and digested with the thrombin to remove the $His_6$ tag. The protein was further purified by anion exchange chromatography using the previously published method for improved SbnA solubility (26). SbnA was dialyzed into 50 mM Tris pH 8, 100 mM NaCl, and 2 mM TCEP, concentrated to approximately 20 mg/mL and stored at -80°C

***Crystallization, data collection, and structure determination of $SbnI^{1-240}$***

Selenomethionine-labeled $SbnI^{1-240}$ crystals were grown by sitting drop vapor diffusion at 4°C in 2 uL drops with a 1:1 mixture of ~20 mg/mL $SbnI^{1-240}$ in 50 mM HEPES (pH 7.4), 100 mM NaCl, 5% (v/v) glycerol, and 2 mM TCEP with reservoir solution containing 0.18 M HEPES (pH 7.5) and 20% (w/v) PEG 8000. Crystals were briefly soaked in reservoir buffer supplemented with 30% (v/v) glycerol for cryoprotection and flash frozen in liquid nitrogen. A single wavelength anomalous diffraction dataset was collected at the Canadian Light Source on Beamline 08B1-1 (57). The data was processed and scaled using XDS (58, 59). Crystals were of space group $P3_1$ with one molecule in the asymmetric unit. Five selenomethionine sites were identified for phasing to build a preliminary model using AutoSol (initial figure of merit of 0.35) and Autobuild (187 of 240 residues built) programs in Phenix (60). Manual building was done using Coot (61) and refinement was performed with phenix.refine using translation liberation screw parameters with

three groups (62). The refined structure contains $Met^{1}$-$Ala^{240}$, one glycerol, and 12 water molecules. Data collection and refinement statistics are summarized in Table 1. Structure figures were generated in PyMOL (The PyMOL Molecular Graphics System, Version 1.8 Schrödinger, LLC). Domain analysis was done using the Dali server for comparison of the protein structure against structures in the PDB (63).

***Genomic neighborhood and conservation analysis***

Protein homology between genomic regions carrying SbnI orthologs was plotted using a custom Biopython script bio.links.py based on output from BLASTP 2.2.2.28 (e-value ≤ 1.00e-40) (https://github.com/minevskiy/bioinformatics). Species used for comparison were found by BLAST search of SbnA or SbnI and STRING analysis of SbnI. Orthologous genes are indicated in the same color.

Sequence conservation was mapped onto the $SbnI^{1-240}$ structure using ConSurf (64). The multiple sequence alignment used for the analysis was generated using default ConSurf parameters and the SbnI amino acid sequence as the search sequence.

***Dynamic light scattering***

Samples of SbnI and $SbnI^{1-240}$ were analyzed by DLS using a DynaPro Plate Reader (Wyatt Technologies). Protein was diluted to 0.5 mg/mL with 50 mM HEPES (pH 7.4), 300 mM NaCl, 5% (v/v) glycerol, and 2 mM GSH and results were generated based on averaging five, 5 second acquisitions. Data were collected at room temperature. Values reported are an average of data collected.

***UV-Vis Spectrophotometry analysis of SbnI OPS production using SbnA***

UV-Vis spectra were collected using Varian Cary 50 UV-Vis spectrophotometer. SbnA-PLP spectrum was recorded at a concentration of 15 µM in 50 mM HEPES pH 7.4, 100 mM NaCl, 5% (v/v) glycerol. The spectrum of SbnA aminoacrylate aldimide complex was recorded immediately after addition of 30 µM OPS (25). The spectral shift observed when SbnA binds OPS was used to evaluate OPS production by SbnI. The spectrum of 15 µM SbnA in 50 mM HEPES pH 7.4, 100 mM NaCl, 5% (v/v) glycerol, 20 mM $MgCl_2$, 25 mM L-serine, and 5 mM ATP was recorded before and after the addition of 15 µM SbnI, SbnI E20A, SbnI D58A, or $SbnI^{1-240}$. Phosphate donor specificity was also examined using 5 mM ADP in place of ATP.

***HPLC***

Kinase activity of SbnI was detected using HPLC to examine production of ADP from ATP. The reaction mixture was composed of 50 mM HEPES (pH 7.4), 100 mM NaCl, 2.5% glycerol, 50 mM L-serine, 0.25 mM ATP or ADP, 10 mM $MgCl_2$, and 5 µM of SbnI, SbnI E20A, or SbnI D58A. The reaction was carried out for 1 hour at room temperature (22ºC). The protein was removed by centrifugation using a 3K nanosep column. The filtrate was 0.2 µm filtered and analyzed by HPLC using a Waters 2695 Separations HPLC module (Milford, MA) equipped with a Waters 2996 photodiode array detector and a Luna 3 µm PFP(2) 50 x 4.6 mm LC column (Phenomenex) using a linear gradient of 0 to 15% methanol in 0.1 M ammonium acetate, pH 4.5 over 10 minutes at 1 mL $min^{-1}$. Analytes were detected by the absorbance at 258 nm.

***$^{31}$P NMR spectra of SbnI kinase reaction***

The reaction mixture contained 50 mM HEPES (pH 7.4), 100 mM NaCl, 2.5% (v/v) glycerol, 10 mM $MgCl_2$, 48 mM L-serine, 5 mM ATP, and 5% $D_2O$. NMR spectra were collected at 25 °C using a broadband frequency probe with Z-magnetic field gradient in a Bruker Avance III 500 MHz spectrometer. One-dimensional $^{31}$P spectra were recorded at different time points before and after addition of 4.8 µM SbnI until reaction completion. The spectra were referenced to 2,2,6,6-tetramethylpiperidine, which was set to 0 ppm. The spectra were processed and using TopSpin™ (Bruker). The chemical shifts of ATP (65) and OPS were assigned using reference spectra (Fig. S3).

***Measurement of serine kinase activity***

ATP-dependent serine kinase activity of SbnI was measured using a pyruvate kinase/lactate dehydrogenase (PK/LDH) coupled assay. The assay is based on a reaction in which

the regeneration of hydrolyzed ATP is coupled to the oxidation of NADH (66). The rate of NADH absorbance decrease at 340 nm ($A_{340\ nm}$ = 6220 $M^{-1}$ $cm^{-1}$) is proportional to the rate of ATP conversion to ADP by SbnI-kinase activity. Coupled reactions contained 50 mM HEPES pH 7.4, 100 mM NaCl, 2.5% (v/v) glycerol, 10 mM $MgCl_2$, 2 mM phosphoenolpyruvate, 1/50 of the final reaction mixture volume of PK/LDH enzyme (from rabbit muscle, Sigma-Aldrich, cat. P-0294), 5 mM ATP, and 100 mM L-serine. The mixture was incubated for 5 min to remove any contaminating ADP. Continuous measurement at 340 nm was recorded for 2 minutes prior to addition of 0.5 μM SbnI, $SbnI^{1-240}$, SbnI E20A, or SbnI D58A enzyme to start the reaction. The assay was run for 10 minutes. To determine kinetic parameters, the initial velocities of SbnI and $SbnI^{1-240}$ kinase reactions in the presence of varying concentrations of ATP with 100 mM L-serine and in the presence of varying concentrations of L-serine with 5 mM ATP were recorded. Phosphate donor specificity was investigated with 10 mM ADP and phosphate acceptor specificity was examined with 50 mM L-threonine, and 50 mM His-Ser dipeptide. In addition, alternative substrates, 50 mM L-Dap and 50 mM α-KG were tested as phosphate acceptors. All data was collected on a Varian Cary 50 UV-Vis spectrophotometer at room temperature (22ºC) and a total of three replicates were collected for each reaction condition.

SbnI kinase activity was also measured using an assay with SbnA. In a reaction mixture, SbnI-dependent OPS production was measured using SbnA and L-glutamate to release inorganic phosphate and *N*-(1-amino-1-carboxyl-2-ethyl)-glutamic acid (26). A coupled enzymatic assay was used to detect inorganic phosphate release from OPS as previously described (67). The reaction mixture contained 50 mM HEPES pH 7.4, 100 mM NaCl, 2.5% (v/v) glycerol, 10 mM $MgCl_2$, 10 mM ATP, 100 mM L-serine, 0.2 U purine nucleoside phosphorylase, 400 μM 2-amino-6-mercapto-7-methylpurine riboside, 5 μM SbnA, 2 mM L-glutamate. The mixture was incubated for 10 min to remove any contaminating inorganic phosphate and establish a baseline. Continuous measurement at 360 nm was recorded for 2 minutes prior to addition of 0.5 μM SbnI or $SbnI^{1-240}$ enzyme to start the reaction. The assay was run for 15 minutes. To determine kinetic parameters, the initial velocities of SbnI kinase reactions in the presence of varying concentrations of ATP with 100 mM L-serine and in the presence of varying concentrations of L-serine with 10 mM ATP were recorded. All data was collected on a Varian Cary 50 UV-Vis spectrophotometer at room temperature (22ºC) and a total of three replicates were collected for each reaction condition. The concentration of inorganic phosphate release from OPS was determined using the extinction coefficient $A_{360\ nm}$ = 11000 $M^{-1}cm^{-1}$ (67). Data were fit by nonlinear regression using a Michaelis-Menten model in GraphPad Prism 6.

### *S. aureus bacterial strains and growth conditions*

Experiments were performed with a derivative of *S. aureus* USA300 LAC cured of the 27-kb plasmid encoding macrolide resistance (68). The plasmid-cured USA300 LAC is referred to as USA300 throughout. Transposon insertion mutants JE2 *serC*::ΦNΣ; $Em^R$ (SAUSA300_1669) and JE2 *sbnI*::ΦNΣ; $Em^R$ (SAUSA300_0126) were obtained from the Nebraska Transposon Mutant Library (NTML) containing the resistance cassette *ermB*, which confers resistance to erythromycin (69). Transposons were transduced to USA300 background strain using phage 80α and confirmed by PCR using published methods (70). USA300 *serC*::ΦNΣ and USA300 *sbnI*::ΦNΣ transposon insertion mutants are referred to as *serC* and *sbnI* throughout (Table 3). Bacterial growth curves to test serine auxotrophy were performed in chemically-defined medium with 0.4% (w/v) glucose (CDMG) as previously described (18), with and without L-serine. Briefly, colonies of wildtype USA300 or *serC* transposon insertion mutant were inoculated from tryptic soy agar into 2 mL CDMG overnight at 37ºC. Cells were normalized to an $OD_{600}$ of 0.1 and washed twice with CDMG lacking L-serine (CDMG-Ser) and 5 μL of the resuspension was used to inoculate 200 μL aliquots of CDMG or CDMG-Ser in 96 well plates. Cultures were grown in TECAN plate reader for 24 hours at 37ºC with 10 second shake every 10 min and the $OD_{600}$ was assessed every 30 min. Data are representative of three independent experiments, and error bars signify standard error of the mean.

***Disc diffusion assays to assess siderophore production***

Concentrated spent culture supernatants were prepared from 10 mL cultures of *S. aureus* USA300, *serC* transposon insertion mutant, and *sbnI* transposon insertion mutant grown for 16 hrs in Chelex-100 treated Tris minimal succinate (TMS), as previously described (71), in a flask to volume ratio of 10:1 at 37ºC with shaking at 200 rpm without antibiotic selection. Growth was assessed via $OD_{600}$ and culture densities normalized. Bacterial cells were pelleted by centrifugation and culture supernatants were filter sterilized and lyophilized overnight. Dried material was resuspended in 0.5 mL sterile $ddH_2O$. To assess growth promotion of concentrated culture supernatants, *S. aureus* strain RN6390 *sirA* mutant (growth of this mutant is dependent on SA in supernatant) or *htsABC* mutant (growth of this mutant is dependent on SB in supernatant) derivatives, as previously described (72), were seeded into TMS agar containing 10 µM ethylenediamine-N, N'-bis(2-hydroxyphenylacetic acid) to 2 x $10^5$ cells/mL. 10 µL of concentrated supernatant was applied to sterile paper discs placed on TMS agar containing the seeded reporter strains, and growth radii about the discs were measured after 24 hr incubation at 37ºC. The reported growth radius has the disc radius (3 mm) subtracted. Statistical analyses conducted using 2-way ANOVA.

**Acknowledgments:**

We thank Kateryna Ievdokymenko for assistance with genomic neighborhood analysis and figure generation. We also thank Dr. Anson Chan for assistance with data collection and Mariko Ikehata and Angele Arrieta for technical assistance. We thank the staff at the CLS for assistance with crystallographic data collection.

This work was supported by the Canadian Institutes of Health Research (CIHR) grants to M.E.P.M (MOP-49597) and D.E.H. (MOP-38002). M.M.V. is supported by a PGSD scholarship from the Natural Sciences and Engineering Research Council. Support for infrastructure for structural biology was provided by the Canadian Foundation for Innovation to M.E.P.M. Research described in this paper was performed using beamlines 08B1-1 and 08ID-1 at the Canadian Light Source, which is supported by the NSERC, the National Research Council Canada, the Canadian Institutes of Health Research, the Province of Saskatchewan, Western Economic Diversification Canada, and the University of Saskatchewan.

The atomic coordinates for the crystal structure of $SbnI^{1-240}$ is available in the Research Collaboratory for Structural Bioinformatics Protein Databank under PDB # 5UJE.

**Conflict of interest:**

The authors declare that they have no conflicts of interest with the contents of this article.

**References**


1. Jones, R. N. (2003) Global epidemiology of antimicrobial resistance among community-acquired and nosocomial pathogens: a five-year summary from the SENTRY Antimicrobial Surveillance Program (1997-2001). *Semin. Respir. Crit. Care Med.* **24**, 121–34
2. Gordon, R. J., and Lowy, F. D. (2008) Pathogenesis of methicillin-resistant *Staphylococcus aureus* infection. *Clin. Infect. Dis.* **46 Suppl 5**, S350-9
3. Lowy, F. D. (1998) *Staphylococcus aureus* Infections. *N. Engl. J. Med.* **339**, 520–532
4. Hammer, N. D., and Skaar, E. P. (2011) Molecular mechanisms of *Staphylococcus aureus* iron acquisition. *Annu. Rev. Microbiol.* **65**, 129–47
5. Sheldon, J. R., and Heinrichs, D. E. (2015) Recent developments in understanding the iron acquisition strategies of gram positive pathogens. *FEMS Microbiol. Rev.* **39**, 592–630
6. Cassat, J. E., and Skaar, E. P. (2013) Iron in infection and immunity. *Cell Host Microbe*. **13**, 509–19
7. Gomme, P. T., and McCann, K. B. (2005) Transferrin: Structure, function and potential therapeutic actions. *Drug Discov. Today*. **10**, 267–273
8. Ratledge, C. (2007) Iron metabolism and infection. in *Food and Nutrition Bulletin*, pp. S515–S523, **28**, S515–S523
9. Grigg, J. C., Ukpabi, G., Gaudin, C. F. M., and Murphy, M. E. P. (2010) Structural biology of heme binding in the *Staphylococcus aureus* Isd system. *J. Inorg. Biochem.* **104**, 341–8
10. Konetschny-Rapp, S., Jung, G., Meiwes, J., and Zähner, H. (1990) Staphyloferrin A: a structurally new siderophore from staphylococci. *Eur. J. Biochem.* **191**, 65–74
11. Haag, H., Fiedler, H. P., Meiwes, J., Drechsel, H., Jung, G., and Zähner, H. (1994) Isolation and biological characterization of staphyloferrin B, a compound with siderophore activity from staphylococci. *FEMS Microbiol. Lett.* **115**, 125–30
12. Beasley, F. C., Marolda, C. L., Cheung, J., Buac, S., and Heinrichs, D. E. (2011) *Staphylococcus aureus* transporters Hts, Sir, and Sst capture iron liberated from human transferrin by Staphyloferrin A, Staphyloferrin B, and catecholamine stress hormones, respectively, and contribute to virulence. *Infect. Immun.* **79**, 2345–2355
13. Dale, S. E., Doherty-Kirby, A., Lajoie, G., and Heinrichs, D. E. (2004) Role of Siderophore Biosynthesis in Virulence of *Staphylococcus aureus*: Identification and Characterization of Genes Involved in Production of a Siderophore. *Infect. Immun.* **72**, 29–37
14. Hanses, F., Roux, C., Dunman, P. M., Salzberger, B., and Lee, J. C. (2014) *Staphylococcus aureus* gene expression in a rat model of infective endocarditis. *Genome Med.* **6**, 93
15. Friedman, D. B., Stauff, D. L., Pishchany, G., Whitwell, C. W., Torres, V. J., and Skaar, E. P. (2006) *Staphylococcus aureus* redirects central metabolism to increase iron availability. *PLoS Pathog.* **2**, e87
16. Malachowa, N., Whitney, A. R., Kobayashi, S. D., Sturdevant, D. E., Kennedy, A. D., Braughton, K. R., Shabb, D. W., Diep, B. A., Chambers, H. F., Otto, M., and DeLeo, F. R. (2011) Global changes in *Staphylococcus aureus* gene expression in human blood. *PLoS One*. **6**, e18617
17. Xu, Y., Maltesen, R. G., Larsen, L. H., Schønheyder, H. C., Le, V. Q., Nielsen, J. L., Nielsen, P. H., Thomsen, T. R., and Nielsen, K. L. (2016) In vivo gene expression in a *Staphylococcus aureus* prosthetic joint infection characterized by RNA sequencing and metabolomics: a pilot study. *BMC Microbiol.* **16**, 80
18. Sheldon, J. R., Marolda, C. L., and Heinrichs, D. E. (2014) TCA cycle activity in *Staphylococcus aureus* is essential for iron-regulated synthesis of staphyloferrin A, but not staphyloferrin B: the benefit of a second citrate synthase. *Mol. Microbiol.* **92**, 824–839
19. Smaldone, G. T., Revelles, O., Gaballa, A., Sauer, U., Antelmann, H., and Helmann, J. D. (2012) A global investigation of the *Bacillus subtilis* iron-sparing response identifies major changes in metabolism. *J. Bacteriol.* **194**, 2594–605
20. Cotton, J. L., Tao, J., and Balibar, C. J. (2009) Identification and characterization of the

*Staphylococcus aureus* gene cluster coding for staphyloferrin A. *Biochemistry*. **48**, 1025–35
21. Cheung, J., Beasley, F. C., Liu, S., Lajoie, G. A., and Heinrichs, D. E. (2009) Molecular characterization of staphyloferrin B biosynthesis in *Staphylococcus aureus*. *Mol. Microbiol.* **74**, 594–608
22. Lamb, A. L. (2015) Breaking a pathogen's iron will: Inhibiting siderophore production as an antimicrobial strategy. *Biochim. Biophys. Acta.* **1854**, 1054–70
23. Cheung, J., Murphy, M. E. P., and Heinrichs, D. E. (2012) Discovery of an iron-regulated citrate synthase in *Staphylococcus aureus*. *Chem. Biol.* **19**, 1568–1578
24. Kobylarz, M. J., Grigg, J. C., Sheldon, J. R., Heinrichs, D. E., and Murphy, M. E. P. (2014) SbnG, a citrate synthase in *Staphylococcus aureus*: a new fold on an old enzyme. *J. Biol. Chem.* **289**, 33797–807
25. Kobylarz, M. J., Grigg, J. C., Takayama, S. J., Rai, D. K., Heinrichs, D. E., and Murphy, M. E. P. (2014) Synthesis of L-2,3-diaminopropionic acid, a siderophore and antibiotic precursor. *Chem. Biol.* **21**, 379–88
26. Kobylarz, M. J., Grigg, J. C., Liu, Y., Lee, M. S. F., Heinrichs, D. E., and Murphy, M. E. P. (2016) Deciphering the Substrate Specificity of SbnA, the Enzyme Catalyzing the First Step in Staphyloferrin B Biosynthesis. *Biochemistry*. **55**, 927–939
27. Laakso, H. A., Marolda, C. L., Pinter, T. B., Stillman, M. J., and Heinrichs, D. E. (2016) A heme-responsive regulator controls synthesis of staphyloferrin B in *Staphylococcus aureus*. *J. Biol. Chem.* **291**, 29–40
28. Skaar, E. P., Humayun, M., Bae, T., DeBord, K. L., and Schneewind, O. (2004) Iron-source preference of *Staphylococcus aureus* infections. *Science*. **305**, 1626–8
29. Erdmann, N., Petroff, T., and Funnell, B. E. (1999) Intracellular localization of P1 ParB protein depends on ParA and *parS*. *Proc. Natl. Acad. Sci. U. S. A.* **96**, 14905–10
30. Chen, B.-W., Lin, M.-H., Chu, C.-H., Hsu, C.-E., and Sun, Y.-J. (2015) Insights into ParB spreading from the complex structure of Spo0J and *parS*. *Proc. Natl. Acad. Sci.* **112**, 6613–6618
31. Nagata, R., Fujihashi, M., Kawamura, H., Sato, T., Fujita, T., Atomi, H., and Miki, K. (2017) Structural Study on the Reaction Mechanism of a Free Serine Kinase Involved in Cysteine Biosynthesis. *ACS Chem. Biol.* **12**, 1514–1523
32. Makino, Y., Sato, T., Kawamura, H., Hachisuka, S. I., Takeno, R., Imanaka, T., and Atomi, H. (2016) An archaeal ADP-dependent serine kinase involved in cysteine biosynthesis and serine metabolism. *Nat. Commun.* **7**, 13446
33. McGuffin, L. J., Bryson, K., and Jones, D. T. (2000) The PSIPRED protein structure prediction server. *Bioinformatics*. **16**, 404–5
34. Ward, J. J., McGuffin, L. J., Bryson, K., Buxton, B. F., and Jones, D. T. (2004) The DISOPRED server for the prediction of protein disorder. *Bioinformatics*. **20**, 2138–9
35. Makino, Y., Sato, T., Kawamura, H., Hachisuka, S.-I., Takeno, R., Imanaka, T., and Atomi, H. (2016) An archaeal ADP-dependent serine kinase involved in cysteine biosynthesis and serine metabolism. *Nat. Commun.* **7**, 13446
36. Maindola, P., Raina, R., Goyal, P., Atmakuri, K., Ojha, A., Gupta, S., Christie, P. J., Iyer, L. M., Aravind, L., and Arockiasamy, A. (2014) Multiple enzymatic activities of ParB/Srx superfamily mediate sexual conflict among conjugative plasmids. *Nat. Commun.* **5**, 5322
37. Jonsson, T. J., Johnson, L. C., and Lowther, W. T. (2009) Protein engineering of the quaternary sulfiredoxin-peroxiredoxin enzyme-substrate complex reveals the molecular basis for cysteine sulfinic acid phosphorylation. *J. Biol. Chem.* **284**, 33305–33310
38. Schumacher, M. A., Tonthat, N. K., Lee, J., Rodriguez-Castañeda, F. A., Chinnam, N. B., Kalliomaa-Sanford, A. K., Ng, I. W., Barge, M. T., Shaw, P. L. R., and Barillà, D. (2015) Structures of archaeal DNA segregation machinery reveal bacterial and eukaryotic linkages. *Science*. **349**, 1120–4
39. Leonard, T. A., Butler, P. J. G., and Löwe, J. (2004) Structural analysis of the chromosome segregation protein Spo0J from *Thermus thermophilus*. *Mol. Microbiol.* **53**, 419–432

40. Jönsson, T. J., Murray, M. S., Johnson, L. C., and Lowther, W. T. (2008) Reduction of cysteine sulfinic acid in peroxiredoxin by sulfiredoxin proceeds directly through a sulfinic phosphoryl ester intermediate. *J. Biol. Chem.* **283**, 23846–51
41. Bhatt, G., and Denny, T. P. (2004) *Ralstonia solanacearum* iron scavenging by the siderophore staphyloferrin B is controlled by PhcA, the global virulence regulator. *J. Bacteriol.* **186**, 7896–904
42. Clarke, S. J., Low, B., and Konigsberg, W. H. (1973) Close linkage of the genes *serC* (for phosphohydroxy pyruvate transaminase) and *serS* (for seryl-transfer ribonucleic acid synthetase) in *Escherichia coli* K-12. *J. Bacteriol.* **113**, 1091–1095
43. Robb, F. T., and Clark, D. S. (1999) Adaptation of Proteins from Hyperthermophiles to High Pressure and High Temperature JMMB Symposium. *J. Molec. Microbiol. Biotechnol*. **1**, 101–105
44. Débarbouillé, M., Dramsi, S., Dussurget, O., Nahori, M.-A., Vaganay, E., Jouvion, G., Cozzone, A., Msadek, T., and Duclos, B. (2009) Characterization of a serine/threonine kinase involved in virulence of *Staphylococcus aureus*. *J. Bacteriol.* **191**, 4070–81
45. Canova, M. J., and Molle, V. (2014) Bacterial Serine/Threonine Protein Kinases in Host-Pathogen Interactions. 10.1074/jbc.R113.529917
46. Halsey, C. R., Lei, S., Wax, J. K., Lehman, M. K., Nuxoll, A. S., Steinke, L., Sadykov, M., Powers, R., and Fey, P. D. (2017) Amino acid catabolism in *Staphylococcus aureus* and the function of carbon catabolite repression. *MBio*. 10.1128/mBio.01434-16
47. Chang, T. S., Jeong, W., Woo, H. A., Sun, M. L., Park, S., and Sue, G. R. (2004) Characterization of mammalian sulfiredoxin and its reactivation of hyperoxidized peroxiredoxin through reduction of cysteine sulfinic acid in the active site to cysteine. *J. Biol. Chem.* **279**, 50994–51001
48. Jeong, W., Sung, J. P., Chang, T. S., Lee, D. Y., and Sue, G. R. (2006) Molecular mechanism of the reduction of cysteine sulfinic acid of peroxiredoxin to cysteine by mammalian sulfiredoxin. *J. Biol. Chem.* **281**, 14400–14407
49. Iglesias-Baena, I., Barranco-Medina, S., Lázaro-Payo, A., López-Jaramillo, F. J., Sevilla, F., and Lázaro, J. J. (2010) Characterization of plant sulfiredoxin and role of sulphinic form of 2-Cys peroxiredoxin. *J. Exp. Bot.* **61**, 1509–1521
50. Zhao, J., Ding, G.-H., Tao, L., Yu, H., Yu, Z.-H., Luo, J.-H., Cao, Z.-W., and Li, Y.-X. (2007) Modular co-evolution of metabolic networks. *BMC Bioinformatics*. **8**, 311
51. Psychogios, N., Hau, D. D., Peng, J., Guo, A. C., Mandal, R., Bouatra, S., Sinelnikov, I., Krishnamurthy, R., Eisner, R., Gautam, B., Young, N., Xia, J., Knox, C., Dong, E., Huang, P., Hollander, Z., Pedersen, T. L., Smith, S. R., Bamforth, F., Greiner, R., McManus, B., Newman, J. W., Goodfriend, T., and Wishart, D. S. (2011) The human serum metabolome. *PLoS One*. **6**, e16957
52. Spahich, N. A., Vitko, N. P., Thurlow, L. R., Temple, B., and Richardson, A. R. (2016) *Staphylococcus aureus* lactate- and malate-quinone oxidoreductases contribute to nitric oxide resistance and virulence. *Mol. Microbiol.* **100**, 759–773
53. Kelly, B., and O'Neill, L. A. (2015) Metabolic reprogramming in macrophages and dendritic cells in innate immunity. *Cell Res.* **25**, 771–784
54. MacPherson, I. S., Rosell, F. I., Scofield, M., Mauk, A. G., and Murphy, M. E. P. (2010) Directed evolution of copper nitrite reductase to a chromogenic reductant. *Protein Eng. Des. Sel.* **23**, 137–45
55. Hames, C., Halbedel, S., Schilling, O., and Stülke, J. (2005) Multiple-mutation reaction: a method for simultaneous introduction of multiple mutations into the *glpK* gene of *Mycoplasma pneumoniae*. *Appl. Environ. Microbiol.* **71**, 4097–100
56. Van Duyne, G. D., Standaert, R. F., Karplus, P. A., Schreiber, S. L., and Clardy, J. (1993) Atomic structures of the human immunophilin FKBP-12 complexes with FK506 and rapamycin. *J. Mol. Biol.* **229**, 105–24
57. Fodje, M., Grochulski, P., Janzen, K., Labiuk, S., Gorin, J., and Berg, R. (2014) 08B1-1: An automated beamline for macromolecular crystallography experiments at the Canadian Light Source. *J. Synchrotron Radiat.* **21**, 633–637

58. Kabsch, W. (2010) XDS. *Acta Crystallogr. Sect. D.* **66**, 125–132
59. Kabsch, W. (2010) Integration, scaling, space-group assignment and post-refinement. *Acta Crystallogr. Sect. D.* **66**, 133–144
60. Adams, P. D., Afonine, P. V, Bunkóczi, G., Chen, V. B., Davis, I. W., Echols, N., Headd, J. J., Hung, L.-W., Kapral, G. J., Grosse-Kunstleve, R. W., McCoy, A. J., Moriarty, N. W., Oeffner, R., Read, R. J., Richardson, D. C., Richardson, J. S., Terwilliger, T. C., and Zwart, P. H. (2010) PHENIX: a comprehensive Python-based system for macromolecular structure solution. *Acta Crystallogr. Sect. D.* **66**, 213–221
61. Emsley, P., and Cowtan, K. (2004) Coot: Model-building tools for molecular graphics. *Acta Crystallogr. Sect. D Biol. Crystallogr.* **60**, 2126–2132
62. Painter, J., and Merritt, E. A. (2006) Optimal description of a protein structure in terms of multiple groups undergoing TLS motion. *Acta Crystallogr. Sect. D Biol. Crystallogr.* **62**, 439–450
63. Holm, L., and Rosenström, P. (2010) Dali server: Conservation mapping in 3D. *Nucleic Acids Res.* **38**, 545–549
64. Ashkenazy H., Erez E., Martz E., P. T. and B.-T. N. (2010) ConSurf 2010: calculating evolutionaly conservation in sequence and structure of proteins and nucleic acids. *Nucleic Acids Res.* **38**, 529–533
65. Cohn, M., and Hughes, T. R. (1960) Phosphorus magnetic resonance spectra of adenosine diphosphate and triphosphate. *I. Eff. pH. J. Biol. Chem.* **235**, 3250–3253
66. Rudolph, F. B., Baugher, B. W., and Beissner, R. S. (1979) Techniques in coupled enzyme assays. *Methods Enzymol.* **63**, 22–42
67. Webb, M. R. (1992) A continuous spectrophotometric assay for inorganic phosphate and for measuring phosphate release kinetics in biological systems. *Proc. Natl. Acad. Sci. U. S. A.* **89**, 4884–7
68. Arsic, B., Zhu, Y., Heinrichs, D. E., and McGavin, M. J. (2012) Induction of the Staphylococcal Proteolytic Cascade by Antimicrobial Fatty Acids in Community Acquired Methicillin Resistant *Staphylococcus aureus*. *PLoS One*. **7**, e45952
69. Fey, P. D., Endres, J. L., Yajjala, V. K., Widhelm, T. J., Boissy, R. J., Bose, J. L., and Bayles, K. W. (2013) A genetic resource for rapid and comprehensive phenotype screening of nonessential *Staphylococcus aureus* genes. *MBio*. 10.1128/mBio.00537-12
70. Novick, R. P. (1991) Genetic Systems in Staphylococci. *Methods Enzymol.* **204**, 587–636
71. Sebulsky, M. T., Speziali, C. D., Shilton, B. H., Edgell, D. R., and Heinrichs, D. E. (2004) FhuD1, a ferric hydroxamate-binding lipoprotein in *Staphylococcus aureus*: A case of gene duplication and lateral transfer. *J. Biol. Chem.* **279**, 53152–53159
72. Beasley, F. C., Vinés, E. D., Grigg, J. C., Zheng, Q., Liu, S., Lajoie, G. A., Murphy, M. E. P., and Heinrichs, D. E. (2009) Characterization of staphyloferrin A biosynthetic and transport mutants in *Staphylococcus aureus*. *Mol. Microbiol.* **72**, 947–63
73. Dale, S. E., Sebulsky, M. T., and Heinrichs, D. E. (2004) Involvement of SirABC in iron-siderophore import in *Staphylococcus aureus*. *J. Bacteriol.* **186**, 8356–62


## FOOTNOTES

The abbreviations used are: SA, staphyloferrin A; SB, staphyloferrin B; NIS, non-ribosomal peptide synthetase-independent siderophore; α-KG, α-ketoglutarate; L-Dap, L-2,3-diaminopropionate; OPS, *O*-phospho-L-serine; PLP, pyridoxal 5'-phosphate; PK/LDH, pyruvate kinase/lactate dehydrogenase; RMSD, root mean square deviation; DLS, dynamic light scattering; TCEP, tris(2-carboxyethyl)phosphine; CDMG, carbon defined medium with glucose; TMS, Tris minimal succinate.

**Tables**

Table 1. Data collection and refinement statistics for SbnI$^{1-240}$.

| | |
|---|---|
| *Data Collection*[a] | |
| Resolution Range (Å) | 42 – 2.50 (2.59 – 2.50) |
| Space group | $P3_1$ |
| Unit cell dimensions | |
| *a*, *b*, *c* (Å) | 55.1, 55.1, 92.7 |
| Unique reflections | 10,883 (1,564) |
| Completeness (%) | 99.9 (100) |
| Redundancy | 2.9 (2.9) |
| Average $I/\sigma I$ | 15.8 (2.2) |
| $R_{merge}$ | 0.051 (1.007) |
| Wilson *B*-factor (Å$^2$) | 56.4 |
| Anisotropy | 0.501 |
| *Refinement* | |
| $R_{work}$ ($R_{free}$) | 0.219 (0.259) |
| Number of water molecules | 12 |
| r.m.s.d. bond length (Å) | 0.003 |
| Average *B*-values (Å$^2$) | 95.0 |
| Ramachandran plot (%) | |
| Most favored regions | 97.5 |
| Disallowed regions | 0.4 |
| PDB ID | 5UJE |

[a]Data collection values in parentheses represent the data for the highest resolution shell.

Table 2. Steady-state kinetic parameters of SbnI and SbnI$^{1-240}$.

| | $K_m$ (mM) | $k_{cat}$ (min$^{-1}$) | $k_{cat}/K_m$ (mM$^{-1}$ min$^{-1}$) |
|---|---|---|---|
| *ATP* | | | |
| SbnI | 0.6 ± 0.1 | 3.9 ± 0.1 | 6.8 ± 1.0 |
| SbnI[a] | 0.2 ± 0.1 | 3.9 ± 0.1 | 17.3 ± 3.6 |
| SbnI$^{1-240}$ | 1.2 ± 0.3 | 2.1 ± 0.1 | 1.7 ± 0.7 |
| *ADP* | | | |
| SerK[b] | 2.4 ± 0.5 | 12240 ± 720 | 5100 |
| *L-serine* | | | |
| SbnI | 340 ± 40 | 14.3 ± 0.8 | 0.04 ± 0.01 |
| SbnI[a] | 150 ± 20 | 10.0 ± 0.6 | 0.07 ± 0.01 |
| SbnI$^{1-240}$ | 900 ± 450 | 2.1 ± 0.1 | 0.02 ± 0.01 |
| SerK[b] | 5.1 ± 0.5 | 13100 ± 300 | 2600 |

[a] Kinetics measured using SbnA coupled assay
[b] Data from Makino *et. al.* (32)

Table 3. Bacterial strains and plasmids used in this study.

| Bacterial strains and plasmids | Description | Source or reference |
|---|---|---|
| Strains | | |
| *E. coli* | | |
| BL21 (λDE3) | F⁻ *ompT gal dcm lon hsdS$_B$* ($r_B^-$ $m_B^+$)λ (DE3 [*lacI lacUV5*-T7 gene 1 *ind1 sam7 nin5*]) | Novagen |
| *S. aureus* | | |
| USA300 | USA300 LAC cured of antibiotic resistance plasmid | (68) |
| JE2 *serC*::ΦNΣ | JE2 *serC*::ΦNΣ; $Em^R$ (SAUSA300_1669) | (69) |
| JE2 *sbnI*::ΦNΣ | JE2 *sbnI*::ΦNΣ; $Em^R$ (SAUSA300_0126) | (69) |
| *serC* | USA300 *serC*::ΦNΣ; $Em^R$ (SAUSA300_1669) | This study |
| *sbnI* | USA300 *sbnI*::ΦNΣ; $Em^R$ (SAUSA300_0126) | This study |
| *sirA* | RN6390Δ*sirA*::$Km^R$; SB transport-deficient mutant | (73) |
| *htsABC* | RN6390Δ*htsABC*:$Tc^R$; SA transport-deficient mutant | (72) |
| Plasmids | | |
| pET28a-*sbnI* | IPTG-inducible expression vector containing *sbnI*; $Km^R$ | This study |
| pET28a-*sbnI*$^{1-240}$ | IPTG-inducible expression vector containing *sbnI*$^{1-240}$; $Km^R$ | This study |
| pET28a-*sbnI-E20A* | IPTG-inducible expression vector containing *sbnIE20A*; $Km^R$ | This study |
| pET28a-*sbnI-D58A* | IPTG-inducible expression vector containing *sbnID58A*; $Km^R$ | This study |

[a] $Em^R$, $Km^R$, and $Tc^R$ designate resistance to erythromycin, kanamycin, and tetracycline respectively.

## Figures

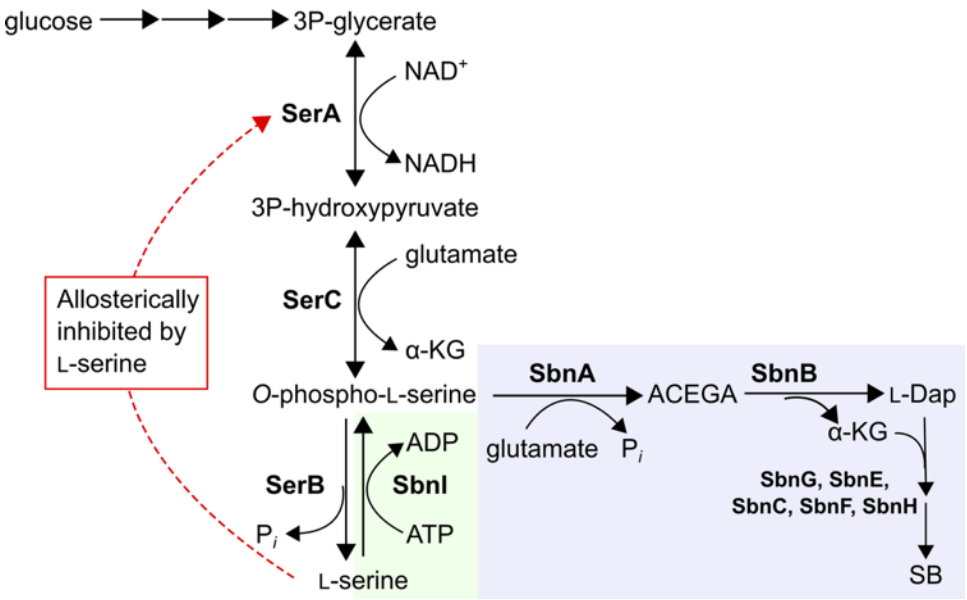


Figure 1. Metabolic pathways for the production of L-Dap and α-KG from glucose or L-serine in *S. aureus*. Highlighted in light green is the contribution of SbnI in this pathway, which feeds into the previously characterized SB biosynthetic pathway (light blue). 3P stands for 3-phospho.

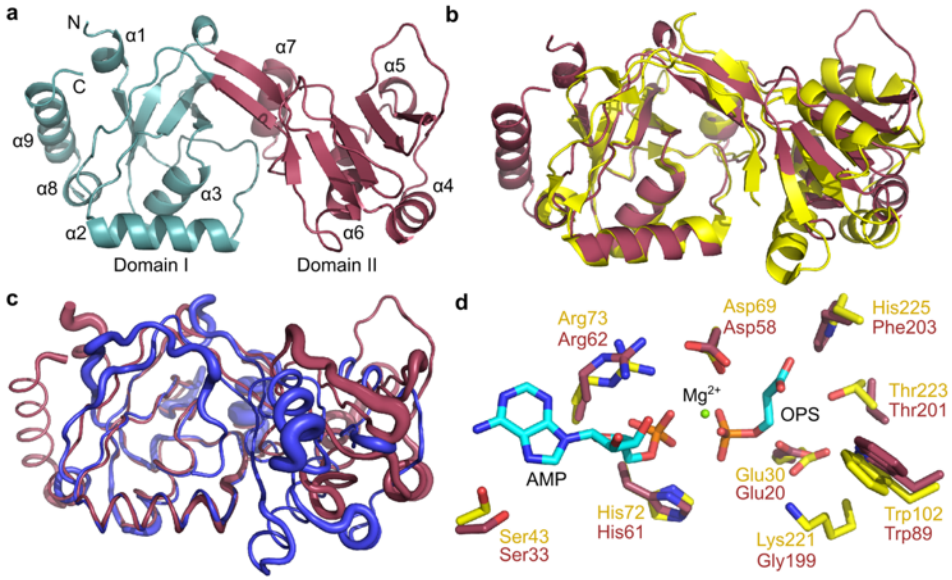


Figure 2. Structure of SbnI$^{1\text{-}240}$. The overall fold of SbnI$^{1\text{-}240}$ is shown as a cartoon and divided into two domains with N- and C-termini and alpha helices labelled. Domain I shown in teal contains the conserved, core ParB/Srx domain (α2 and α3) and domain II is colored raspberry. (B) Structural superimposition of SbnI$^{1\text{-}240}$ (raspberry), and the "open" conformation of SerK (yellow, PDB ID: 5X0B). (C) Superimposition with the "closed" conformation of SerK (blue, PDB 5X0E) in cartoon putty representation, where the size of the tube depends on the B-factor in each structure. (D) Structural superimposition of SaSbnI$^{1\text{-}240}$ (raspberry), and SerK (yellow, PDB ID: 5X0E). Selected active site residues, AMP, and OPS are drawn as sticks. $Mg^{2+}$ is drawn as a green sphere, O, N, and P atoms colored red, blue, and orange, respectively. AMP and OPS carbons are colored cyan.

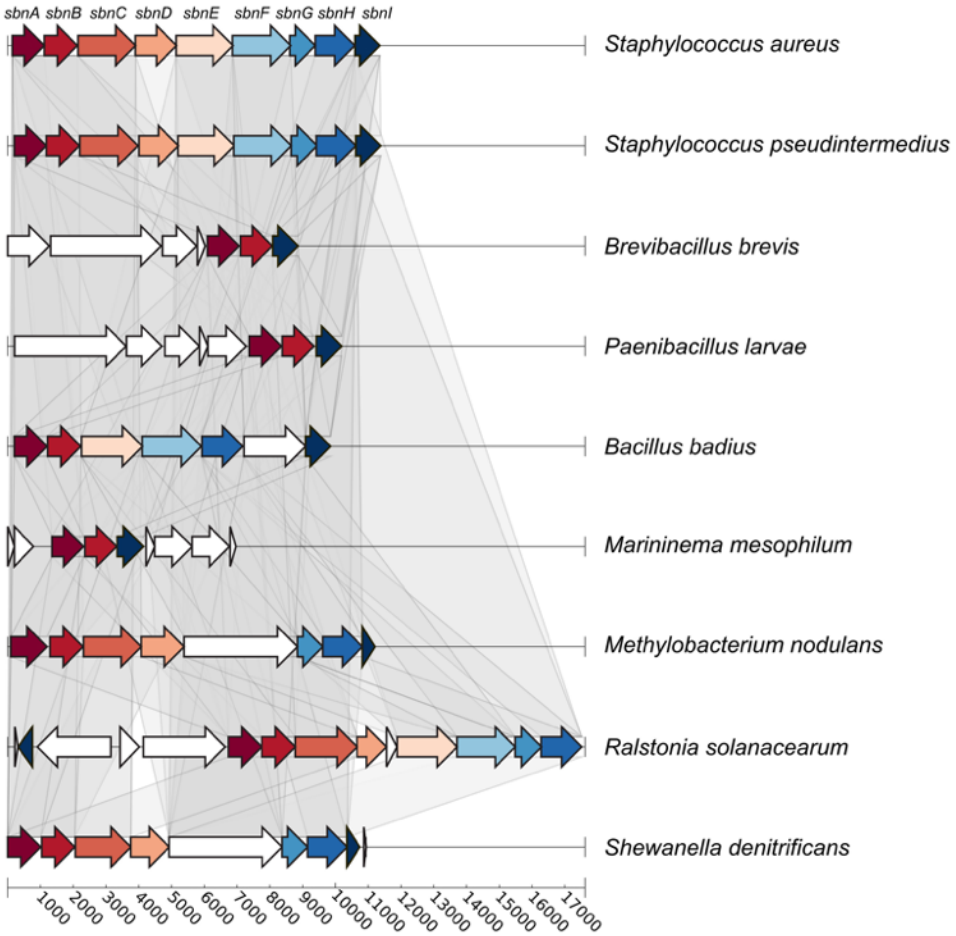


Figure 3. Illustration of gene neighborhoods containing SbnI homologs from diverse species from Firmicute and Proteobacteria phyla. Each predicted gene is represented by an arrow showing the direction of transcription. Grey links connect protein homologous with e-value≤1e-40 and orthologous genes are indicated in the same color. This figure highlights that SbnI homologs appear in the same genomic context as SbnA and SbnB homologs in these bacterial genomes. The bottom scale shows the length of depicted genomic regions in nucleotide base pairs. Region coordinates used for each species are as follows (GenBank:nucleotide region): *Staphylococcus aureus* USA300 FPR3757 (CP000255.1:134324-145881), *Staphylococcus pseudintermedius* E104 (LAWU01000001.1:151604-163186), *Brevibacillus badius* NBRC 110488 (NZ_BDFB01000004.1:355053-396579), *Paenibacillus larvae* SAG 10367 (NZ_CP020557.1:4429364-4439754), *Bacillus badius* DSM 5610 (NZ_LVTO01000018.1:5060-15111), *Marininema mesophilum* DSM 45610 (NZ_FNNQ01000001.1:200002-206967), *Methylobacterium nodulans* ORS 2060(NC_011894.1:7032971-7044380), *Ralstonia solacearum* CQPS-1 (NZ_CP016915.1:169574-186973), and *Shewanella denitrificans* OS217 (NC_007954.1:663307-674451).

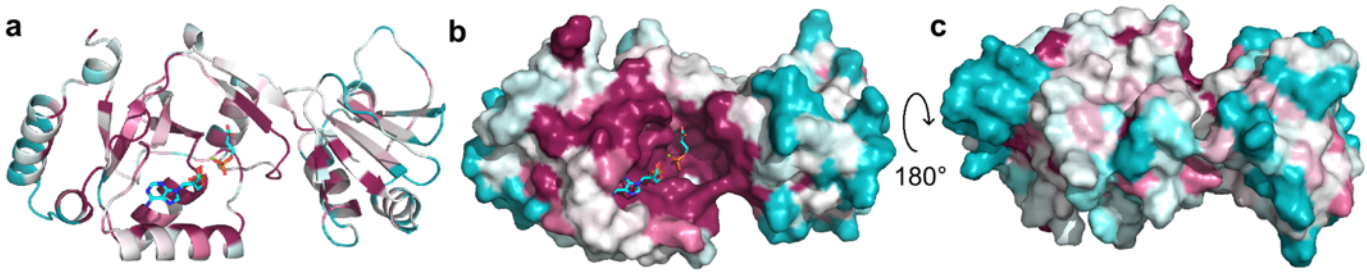


Figure 4. Conservation of surface residues of SbnI$^{1-240}$ generated using ConSurf. (A, B) Ribbon and surface representations of SbnI$^{1-240}$ have AMP and OPS modelled based on a structural alignment with the SerK ternary product complex (PDB ID: 5X0E). (C) Surface representation of SbnI$^{1-240}$ after 180° rotation about the x-axis. Conserved amino acids are colored maroon, residues of average conservation are white, and variable amino acids are turquoise.

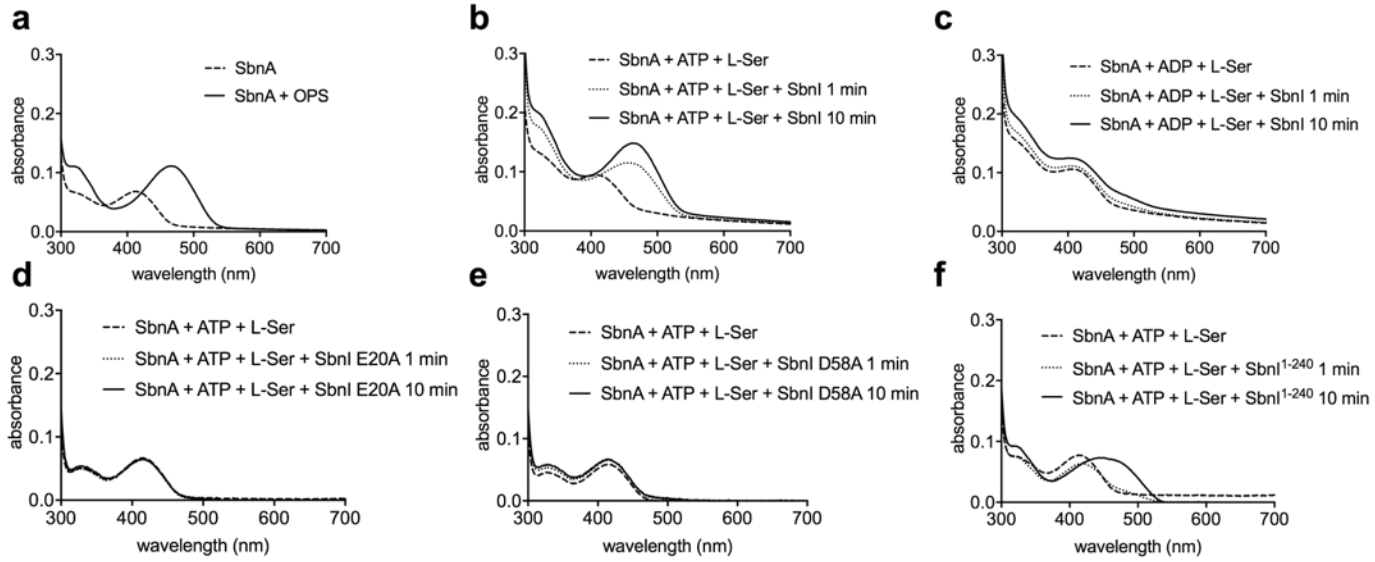


Figure 5. Detection of OPS by SbnI via reaction with SbnA. (A) UV-visible absorption spectra of SbnA and SbnA in complex with OPS. (B) Spectra of SbnA incubated with SbnI-generated OPS from L-serine and ATP but not (C) ADP. SbnI variants (D) E20A and (E) D58A are defective in producing OPS as indicated by no change in the SbnA absorption spectra. (F) SbnI$^{1-240}$ is capable of producing OPS but at a slower rate compared to full-length SbnI.

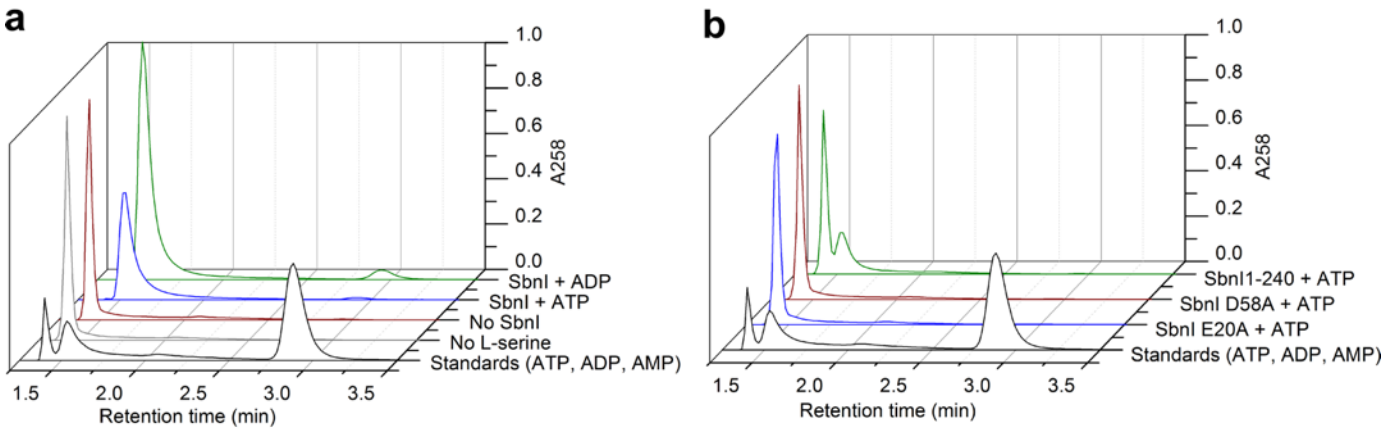


Figure 6. HPLC analysis of the nucleotide reaction products. HPLC trace of ATP, ADP, and AMP standards (black lines) with retention times 1.4, 1.5, and 2.9 min, respectively. (A) SaSbnI, L-serine, and ADP (green line) or ATP (blue line), control reactions of ATP and L-serine excluding SbnI (red line) and of SbnI and ATP excluding L-serine (grey line). (B) Reactions of variants SaSbnI$^{1\text{-}240}$ (green line), SbnI D58A (red line), or SbnI E20A (blue line) with ATP and L-serine.

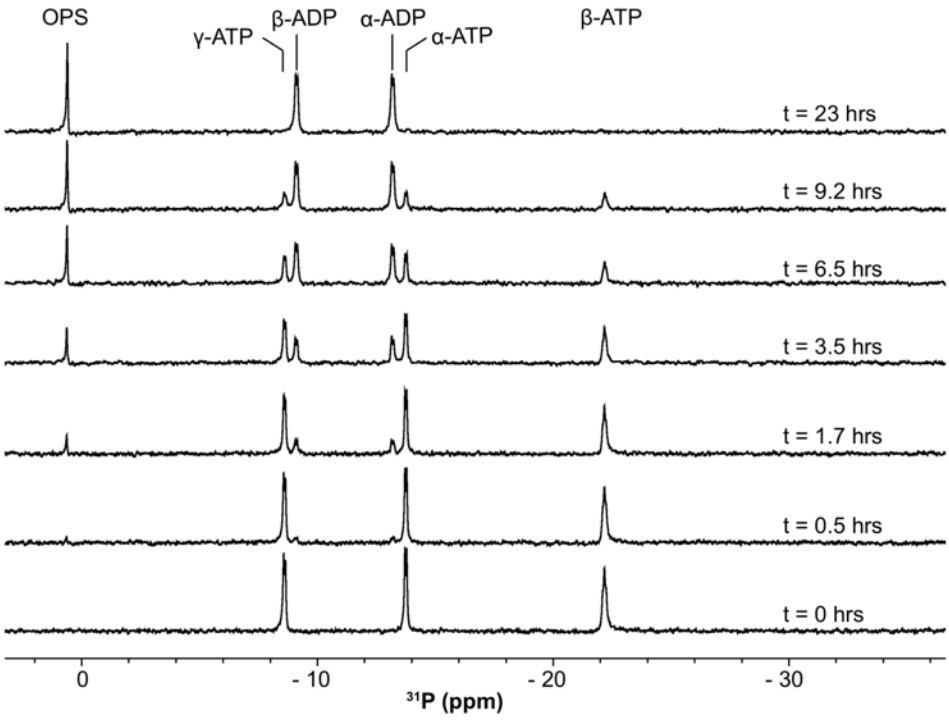


Figure 7. A stack plot of $^{31}$P NMR spectra for a single reaction of SbnI mediated conversion of L-serine and ATP to OPS and ADP. The reaction was initiated by the addition of SbnI with a final concentration of 4.8 μM. The initial concentrations of ATP and L-serine were 5 and 48 mM, respectively. The reaction buffer contained 50 mM HEPES pH 7.4, 100 mM NaCl, 10 mM $MgCl_2$, and 2.5% (v/v) glycerol.

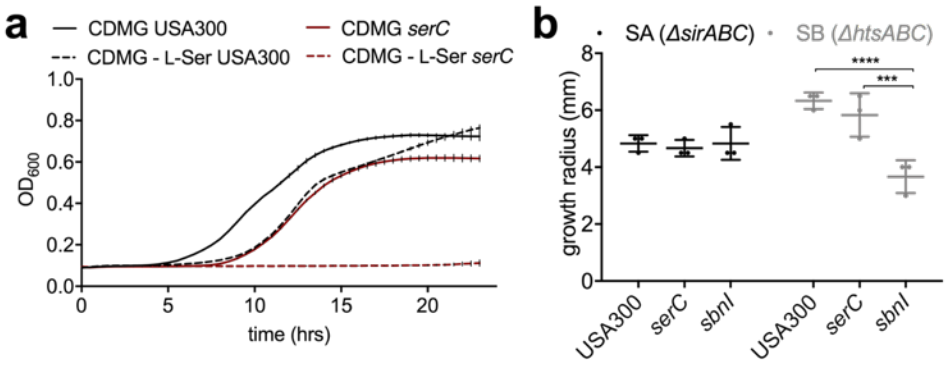


Figure 8. (A) Growth kinetics of *S. aureus* USA300 wildtype (black lines) and *serC* transposon insertion mutant (red lines) strains in chemically defined medium with glucose (CDMG) (solid lines) and CDMG without L-serine (CDMG – L-Ser) (dashed lines). (B) Agar plate disc diffusion bioassays were performed using culture supernatants prepared from *S. aureus* USA300 strains (wildtype and *sbnI* and *serC* transposon insertion mutants), as indicated on the x-axis, that were grown for 16 hrs in chelex-treated Tris minimal succinate (c-TMS) media. The black dots [labeled SA (*ΔsirA*)] are a measure for the presence of SA in culture supernatants and the grey dots [labeled SB (*ΔhtsABC*)] are a measure of SB in culture supernatants based on the growth radius around the disc. The disc radius (3 mm) is subtracted from the reported growth radius. Lines represent the standard deviation from the mean. *** p-value < 0.0002, **** p-value < 0.0001.

**SbnI is a free serine kinase that generates *O*-phospho-L-serine for staphyloferrin B biosynthesis in *Staphylococcus aureus***

Meghan M. Verstraete, Cecilia Perez-Borrajero, Kirstin L. Brown, David E. Heinrichs and Michael E. P. Murphy

*J. Biol. Chem. published online February 26, 2018*

---